

Origin of the drastic decrease of fusion probability in superheavy mass region

Yoshihiro Aritomo^a Masahisa Ohta^b

^a*Flerov Laboratory of Nuclear Reactions, JINR, Dubna, Russia*

^b*Department of Physics, Konan University, 8-9-1 Okamoto, Kobe, Japan*

Abstract

The fusion-fission process in the superheavy mass region is studied systematically by solving the time evolution of nuclear shape in three-dimensional deformation space using the Langevin equation. By analyzing the trajectory in the deformation space, we identify the critical area when the trajectory's destination is determined to be the fusion or the quasi-fission process. It is also clarified that the potential landscape around the critical area is crucial for estimating the fusion probability, and its dependence on the atomic number is presented.

Key words: superheavy elements, fusion hindrance, fluctuation-dissipation dynamics, fusion process, quasi-fission process

1 Introduction

The fusion reaction in which two nuclei combine shows a variety of phenomena controlled by properties inherent in light to heavy nuclei. In the fusion reaction in which a compound nucleus with atomic number $Z < 70$ is formed, the cross section of the reaction can be described by the critical distance model (1) based on the strong absorptive nature of nuclei when they approach each other to within the contact distance where the configuration is more compact than that of the saddle shape for fission. For the region of atomic number $70 < Z < 90$, however, the critical distance model breaks down due to the effect of dissipation force near the contact area, and therefore the extra-push model is proposed (2; 3). The term *fusion hindrance* is focused on this extra-push model. In addition to dissipation, when the atomic number increases beyond 100, the geometrical inversion between the contact point of two nuclei and the saddle point of the composite system substantially affects the fusion probability (4; 5). Therefore, since the saddle point is located inside the contact

point, it is expected that the essential factor for fusion hindrance is strongly related with the landscape of the region in which two nuclei are considerably overlapping.

In this paper, we show how the fusion hindrance should be described in heavy and superheavy nuclei with the region $Z > 100$. In the region, due to the strong Coulomb repulsion force, the shape of the fragment of fissioning nucleus is easily deformed in the fusion-fission process. Therefore, it is extremely important to take into account the deformation of the fragments. The fusion probability in the superheavy mass region has already been reported in references (6; 7; 8) taking account of the fragment deformation. On the basis of the results of our previous studies, we here present the origin of the fusion hindrance as determined by the analysis of the dynamical evolution of nuclear shape during the fusion process.

Generally, the stability for fission in heavy nucleus is discussed on the fission barrier height, which is calculated, for example, by the liquid drop model and the shell correction energy. In the liquid drop part, we can understand the general tendency of the fission life time which decreases exponentially with increasing the atomic number of the nucleus. On the other hand, we can understand the irregularity of the nuclear property by the shell correction energy, and explain the enhancement of the stability of the superheavy mass nucleus. In the same way, the fusion process should be discussed both in the macroscopic point of view and the microscopic one. Even though the fusion barrier is modified by the shell effect, the extent of the fusion enhancement due to the shell effect is depends on the system, namely the potential landscape around the contact point. This is still an open problem and in this paper we restricted to discuss the major part of the fusion hindrance coming from the macroscopic potential. However, we remark that how the shell effect modify the trend of the hindrance due to the macroscopic potential.

In section 2, we briefly explain our framework for the study and the model. We investigate the fusion hindrance precisely in section 3. In this section, we discuss the stability of the deformation in superheavy mass nuclei, and present how the fusion hindrance appears with increasing the atomic number of the colliding partner, using the mean trajectory calculation. The critical condition of the fusion process is discussed. Fusion probability is calculated by the three-dimensional Langevin equation and the role of the shell effect in the fusion process is discussed. In section 4, we present a summary and further discussion to clarify the reaction mechanism in the superheavy mass region.

2 Model

Using the same procedure as described in reference (7), to investigate the fusion-fission process dynamically, we use the fluctuation-dissipation model and employ the Langevin equation for the estimation of fusion probability. We adopt the three-dimensional nuclear deformation space given by two-center parameterization (9; 10) and the time evolution of the nuclear shape is calculated by Langevin equation (we call it *trajectory* in the deformation space). The three collective parameters involved in the calculation are as follows: z_0 (distance between two potential centers), δ (deformation of fragments) and α (mass asymmetry of the colliding nuclei); $\alpha = (A_1 - A_2)/(A_1 + A_2)$, where A_1 and A_2 denote the mass numbers of the target and the projectile, respectively. We assume that each fragment has the same deformation as the first approximation. The neck parameter ϵ is defined in the same manner as reference (9). In the present calculation, ϵ is fixed to be 1.0, so as to retain the contact-like configuration more realistically for two-nucleus collision. The multidimensional Langevin equation is given as

$$\begin{aligned} \frac{dq_i}{dt} &= (m^{-1})_{ij} p_j, \\ \frac{dp_i}{dt} &= -\frac{\partial V}{\partial q_i} - \frac{1}{2} \frac{\partial}{\partial q_i} (m^{-1})_{jk} p_j p_k - \gamma_{ij} (m^{-1})_{jk} p_k + g_{ij} R_j(t), \end{aligned} \quad (1)$$

where a summation over repeated indices is assumed. q_i denotes the deformation coordinate specified by z_0 , δ and α . p_i is the conjugate momentum of q_i . V is the potential energy, and m_{ij} and γ_{ij} are the shape-dependent collective inertia parameter and dissipation tensor, respectively. A hydrodynamical inertia tensor is adopted in the Werner-Wheeler approximation for the velocity field, and the wall-and-window one-body dissipation is adopted for the dissipation tensor (11; 12; 13). The normalized random force $R_i(t)$ is assumed to be white noise, *i.e.*, $\langle R_i(t) \rangle = 0$ and $\langle R_i(t_1) R_j(t_2) \rangle = 2\delta_{ij} \delta(t_1 - t_2)$. The strength of random force g_{ij} is given by $\gamma_{ij} T = \sum_k g_{ij} g_{jk}$, where T is the temperature of the compound nucleus calculated from the intrinsic energy of the composite system. The potential energy is defined as

$$V(q, l) = V_{DM}(q) + \frac{\hbar^2 l(l+1)}{2I(q)}, \quad (2)$$

$$V_{DM}(q) = E_S(q) + E_C(q), \quad (3)$$

where $I(q)$ is the moment of inertia of a rigid body at deformation q V_{DM} is the potential energy of the finite-range liquid drop model. E_S and E_C denote a generalized surface energy (14) and Coulomb energy, respectively. The cen-

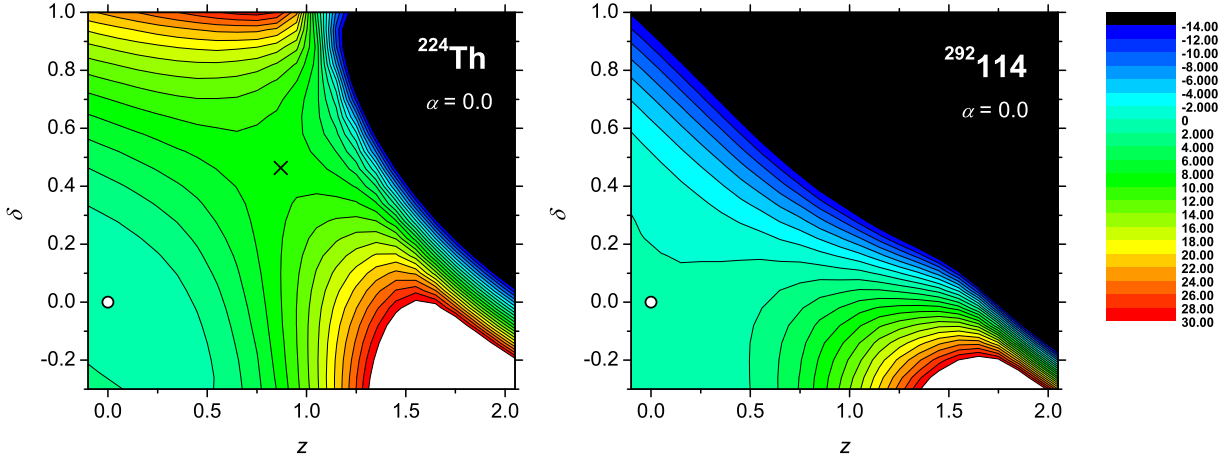


Fig. 1. The potential energy surface of a liquid drop model on the $z - \delta$ plane for ^{224}Th (left) and $^{292}\text{114}$ (right). The mass asymmetric parameter α is zero. The saddle point marked by \times is well observed in the case of ^{224}Th . The stability of the spherical nucleus, marked by circles, against the parameter δ can be seen for Th but not for the nucleus with $Z=114$.

trifugal energy arising from the angular momentum l of the rigid body is also considered. The detail is explained in reference (7).

3 Origin of the fusion hindrance in superheavy mass region

3.1 Role of the nuclear deformation

Figure 1 shows the potential energy surface of the liquid drop model (*LDM*) for ^{224}Th (left) and $^{292}\text{114}$ (right) on the $z - \delta$ plane with angular momentum $l = 0$ and symmetry $\alpha = 0$. This potential energy surface is calculated using the two-center shell model code (15; 16). The contour lines of the potential energy surface are drawn in steps of 2 MeV. As described in reference (7), to save computational time, we use scaling and employ the coordinate z . The coordinate z is defined as $z = z_0/(R_{CN}B)$, where R_{CN} denotes the radius of the spherical compound nucleus. Parameter B is defined in terms of the fragment deformation parameter δ as $B = (3 + \delta)/(3 - 2\delta)$. In Fig. 1, the position at $z = \delta = 0$ corresponds to a spherical compound nucleus marked by the circle (o).

For ^{224}Th , we can see the pocket located in the spherical region and the nucleus in this pocket is rather stable being protected by the well-defined fission barrier marked by the cross (\times). On the other hand, for $^{292}114$, no fission barrier can be seen when the shell effect is not taken into account, and the nucleus around the spherical region is unstable against fragment deformation, as shown in Fig.1, due to the Coulomb force acting between two centers. That is, the system tends to rupture easily, which induces fragment deformation competing with the shell effect. The instability of the superheavy nucleus has been discussed from the viewpoint of the fission barrier due to the shell effect along the z -direction, but we have never paid attention to the fragment deformation parameter δ under the condition of small variation in z . Particularly in the synthesis of the superheavy elements, when we treat the fusion process, the fragility of the composite system with respect to δ is crucial, because, as mentioned in Introduction, the saddle point for fission is far inside the contact configuration, and the instability due to the fragment deformation is easily realized.

3.2 Characteristics of the mean trajectories

First, we want to clarify how the critical condition changes upon separating the trajectory for fusion and that for quasi-fission when the atomic number of the compound nucleus increases. In order to see the fundamental variation of the critical condition, we employ the potential energy of the liquid drop model, and calculate the mean trajectory. That is to say, we delete the final term on the right-hand side of Eq. (1). We want to exclude the influence of the individuality of each nuclei. In this stage, the shell effect is not taken into account considering that the shell effect on the fusion probability is expected to cause the fluctuation around the mean trajectory on the liquid drop potential, and it is better to understand the fundamental systematics of fusion hindrance. Actually, we discuss the fusion probability including the shell effect in subsection 3.4.

Figure 2 shows the mean trajectory for forming the compound systems ^{224}Th , ^{232}Pu , ^{240}Cf , ^{256}No , ^{267}Sg , ^{280}Ds , $^{292}114$ and $^{297}118$, which are produced by hot fusion reaction. For all systems, the entrance channel is chosen to have the same mass asymmetry, $\alpha = 0.6$, and the incident energy corresponding to the excitation energy of the compound nucleus $E^* = 50$ MeV. The mean trajectory for $l = 0$ is projected onto the $z - \alpha$ ($\delta = 0$) and $z - \delta$ ($\alpha = 0$) planes in Figs. 2(a) and (b), respectively. The trajectory calculation starts at the point of contact located at $(z, \delta, \alpha) = (1.56, 0.0, 0.6)$ indicated by the arrow.

The above-mentioned mean trajectories are grouped into two parts, that is,

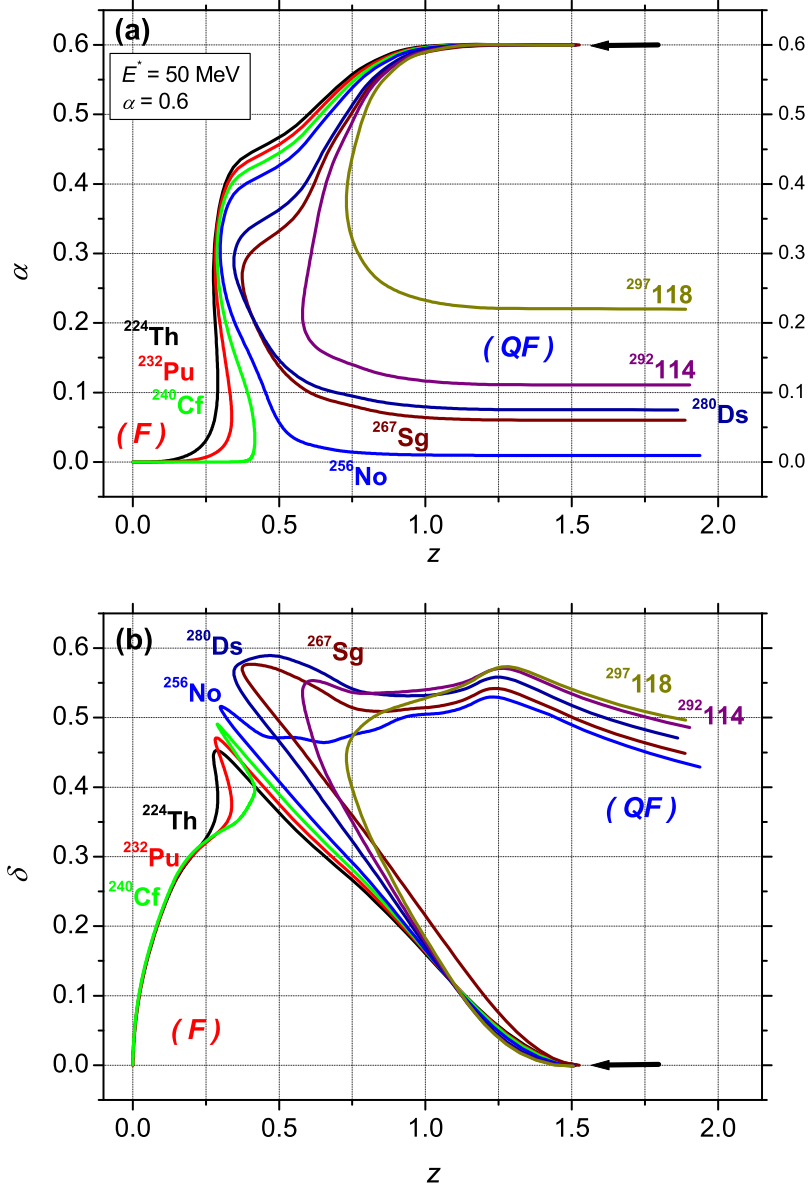


Fig. 2. The mean trajectories for forming various compound systems. The entrance channels are chosen to have $\alpha = 0.6$ and $E^* = 50$ MeV. The mean trajectories are projected onto the (a) $z-\alpha$ ($\delta = 0$) plane and (b) $z-\delta$ ($\alpha = 0$) plane. The starting point of the calculation is $(z, \delta, \alpha) = (1.56, 0.0, 0.6)$, which is indicated by arrows. The trajectory is classified into two groups: one leading to fission (marked by F) and the other leading to quasi-fission (marked by QF).

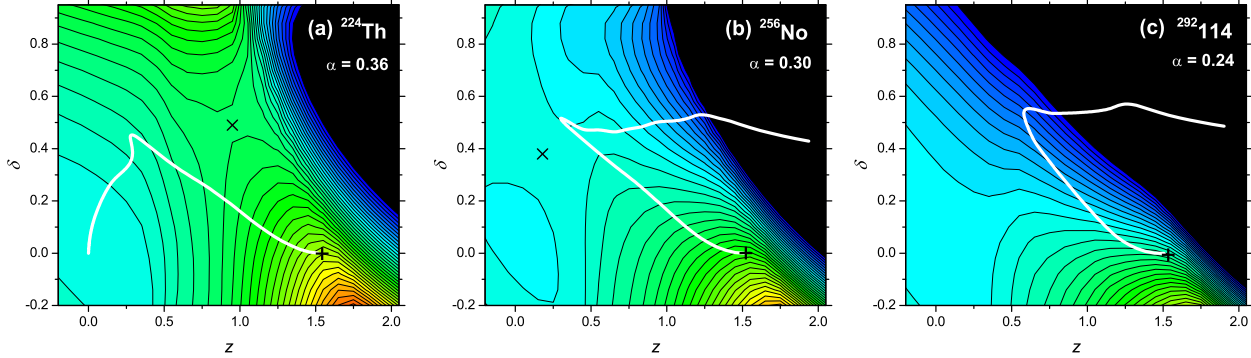


Fig. 3. The potential energy surfaces on the $z - \delta$ plane for (a) ^{224}Th , (b) ^{256}No and (c) $^{292}\text{114}$. The mass asymmetry parameter α is chosen as the value for each critical area. The mean trajectory projected onto the $z - \delta$ plane is drawn by the white line. The initial point is marked by $+$. We define the area where the direction of the trajectory drastically changes as the critical area.

the fusion (F) and the quasi-fission (QF) process. On the $z - \alpha$ plane, for the trajectories of $Z = 90, 94$ and 98 systems, the mass asymmetry parameter α relaxes quickly in the region of small z , and ultimately, the trajectories go to the spherical region. The trajectory of the $Z = 102$ system at first arrives in the area of $z \sim 0.3$, goes to the positive z direction and then finally moves to mass symmetric fission. With increasing atomic number of the system, it becomes increasingly difficult for the trajectory to reach the smaller z region and it ultimately returns to the mass asymmetric fission region. We can see the tendency that the mass asymmetry of fission fragments increases with increasing atomic number of the reaction system, which is consistent with the experimental data presented by Bock et al. (17).

The situation can be understood by examining the characteristic behavior of the trajectories projected onto the $z - \delta$ plane, as shown in Fig. 2(b). As discussed in references (7; 8), the fragment deformation parameter δ plays a very important role in the fusion-fission process in the superheavy mass region. Even for the $Z < 102$ system, the mean trajectory at first goes to the positive δ direction but the direction changes to the negative δ direction and reaches to the spherical region.

All trajectories go to the positive δ direction from the point of contact, and change their direction at around $\delta \sim 0.5$. This trend is common for all systems treated here and we call this area the *critical area*. In systematic investigation, we can see that the behavior of the trajectory in the critical area is the key in deciding whether it becomes the fusion process or the quasi-fission process.

The potential landscape in the critical area is strongly related with the fusion probability, as we discuss later.

3.3 Critical condition of fusion process

In order to understand the difference appearing in the trajectories of fusion and quasi-fission processes, we again investigate the landscape of the potential energy surface on the $z - \delta$ plane. Figures 3(a), (b) and (c) show the potential energy surface with the trajectory for forming ^{224}Th , ^{256}No and $^{292}\text{114}$, respectively. These are drawn by the cross section at the parameter α close to the critical area which is indicated in the figure. The white line denotes the mean trajectory and the initial point is marked by (+).

For ^{224}Th , the potential barrier develops well at large δ . In the critical area, the mean trajectory automatically descends to the spherical region along the potential slope. We can still see the saddle point marked by (\times) in this system. Here, the critical area for the mean trajectory is located just inside the saddle point. Therefore, the fusion process is predominant. On the other hand, for $Z > 102$ systems, the critical area is outside the saddle point even if it is still observed and no potential barrier can be seen at large δ , as shown in Figs. 3(b) and (c). The critical area is located almost midway on the slope leading to fission.

The critical situation can clearly be seen when we plot the cross section of the potential energy surface around the critical area. Figure 4 shows the one-dimensional potential energy surface depending on δ , with fixed $z = 0.3$ and $\alpha = 0.3$. The gradient of the potential energy surface changes from positive to negative at $Z = 102$. This feature is the essential factor for the mean trajectory whether it follows the fusion process or the quasi-fission process.

As can be seen from Fig.3, the mean trajectory on the $z - \delta$ plane seems to stop for a moment at the critical area. The mass asymmetry parameter α relaxes drastically at this moment, as shown in Fig. 2(a). When the slope of the potential in the critical area is relatively gentle, the trajectory spends a long time here and the mass asymmetry easily relaxes. On the other hand, when the slope in the critical area is steep toward the fission region, the residence time of trajectory is too short for relaxing the mass asymmetry completely, and the trajectory goes to the mass asymmetric fission (or quasi-fission) region.

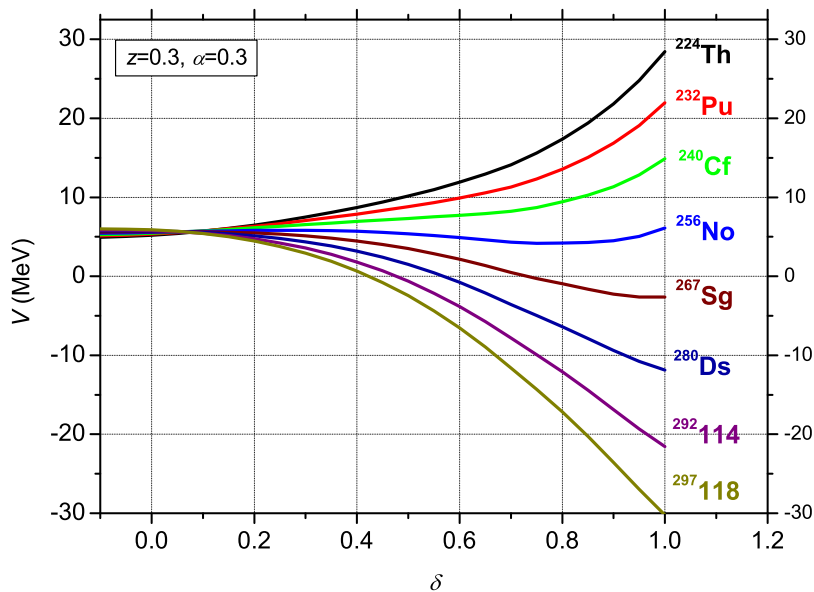


Fig. 4. One-dimensional potential energy surface of the various systems depending on δ , with fixed $z = 0.3$ and $\alpha = 0.3$. It roughly corresponds to the cross section of the potential energy surface in the critical area. The stability of the composite nucleus against δ changes in ^{256}No .

3.4 Fusion probability forming superheavy elements

Next, we discuss the systematics of the fusion probability using the fluctuation-dissipation model. Using the same procedure as described in reference (7), we calculate the fusion probability taking into account the fluctuation around the mean trajectory. Figure 5 shows the results for each system, in the case of $l = 0$. The calculations are performed for the case of two entrance channel mass asymmetries, $\alpha = 0.6$ and 0.0 . In Fig. 5(a), since the mean trajectories for $Z = 90, 94$ and 98 systems are classified as fusion processes, the fusion probability is almost unity even if the fluctuation effect is taken into account. For $Z > 102$ systems, the fusion probability decreases exponentially with increasing Z number.

It is strongly related to the landscape of the potential energy surface. With decreasing entrance channel mass asymmetry, the fusion probability decreases due to the relationship between the ridge line on the $z - \delta$ plane and the point where the kinetic energy dissipates, as mentioned in reference (8). When the initial value is $\alpha = 0$, the fusion probability becomes smaller, because the distance between the ridge line on the $z - \delta$ plane and the point where the kinetic energy dissipates is large.

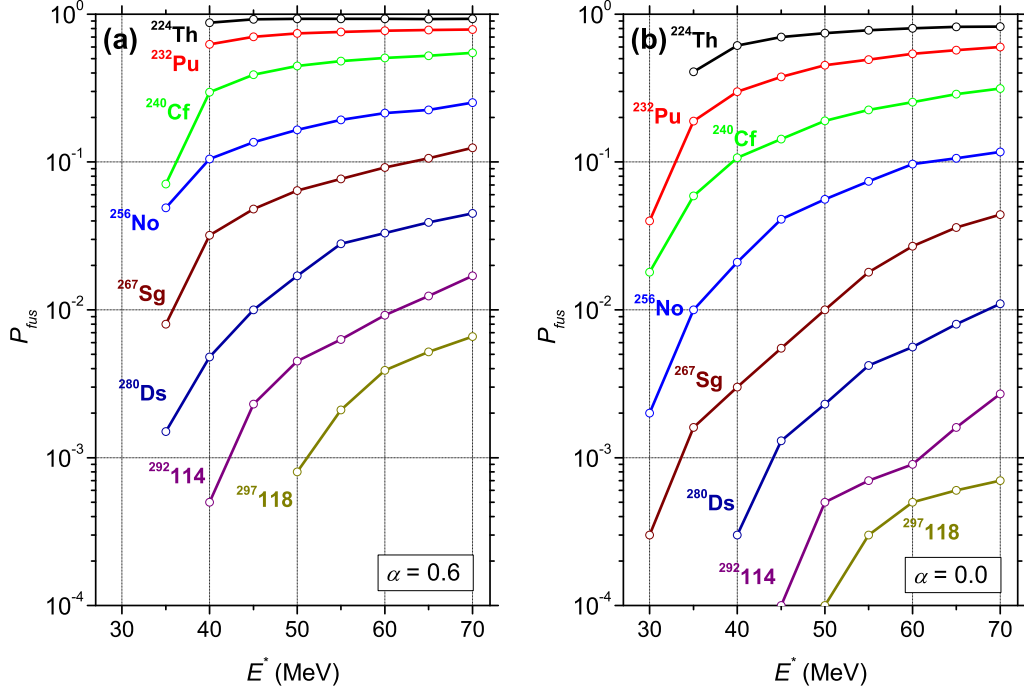


Fig. 5. Fusion probability for each system calculated using the fluctuation-dissipation model, in the case of $l = 0$. The initial conditions are (a) $\alpha = 0.6$ and (b) $\alpha = 0.0$.

Though we discussed the general aspect of the fusion process using the macroscopic model, in order to compare the calculations with the experimental data, we should consider the shell effect in fusion process, as we mentioned in Introduction. The shell effect plays a very important role and enhances sometime the fusion probability (fusion enhancement) (18; 19; 20; 21). Here, we calculate the fusion probability taking into account the shell correction energy for the potential energy surface.

In the cold fusion reaction, Pb target is chosen to suppress the excitation energy of compound nucleus (22). Due to the strong shell structure of Pb target, the potential energy at the contact point of the system is smaller than that of only the liquid drop model. Moreover, the fusion valley ("cold valley") which originates by the shell effect leads to enhance the fusion probability (18; 21; 7; 8). We calculate the fusion probability for $l = 0$ in the potential energy surface of the *LDM* and *LDM* with the shell correction energy, which are shown in Fig. 6 (a) and (b), respectively. As an initial condition, we use the

combination of the cold fusion reaction. In the calculations shown in Fig. 6(b), we use the full shell correction energy for the potential energy surface, though the shell correction energy depends on the nuclear temperature T . This is our intentional way to demonstrate the role of the shell correction energy in the dynamical process.

When we take into account the shell correction energy in the potential energy surface, the fusion probability increases for all systems. The shell correction energy changes the potential landscape, and it becomes easy for the trajectory to reach the fusion region, which has been discussed precisely in reference (7; 8). For $Z < 102$ in Fig. 6, the fusion probability shows the almost unit.

In order to calibrate our calculation, we compare our results with the experimental data in the cold fusion reactions. Figure 7 shows the fusion probability on Pb-target reaction series. We plot the experimental data (23) at the excitation energy corresponding the Bass barrier height (24) by open squares. The calculation for $l = 0$ is denoted by solid circles. The fusion hindrance are seen from $Z_1 \times Z_2 > 1750$, where Z_1 and Z_2 denote the atomic number of the target and projectile, and the fusion probability decreases drastically. The tendency of the experimental data is reproduced by our calculation.

We have discussed the mechanism of the dynamical process in the case of $l = 0$. When the system has an angular momentum, the potential landscape changes, and the absolute value of the fusion probability changes. However, the general tendency of the fusion probability for each system is very similar in any angular momentum cases.

4 Summary

The fusion-fission process in the superheavy mass region was studied systematically by the trajectory calculation in the three-dimensional coordinate space. In order to see the systematics clearly, we employed the potential energy of the liquid drop model, and calculated the mean trajectory. We investigated the mechanism of the occurrence of fusion hindrance by increasing the atomic number of the system. The mean trajectory for all systems treated here at first goes to the positive δ direction. Then, the gradient of the δ direction of the potential energy surface in the critical area governs whether the mean trajectory becomes the fusion or the quasi-fission process. The fusion probability is consequently estimated from the diffusion along the mean trajectory. From the behavior of the mean trajectory shown in Fig. 3, we can understand that the fusion probability decreases exponentially as the Z number of the fused system increases. It is concluded that the fusion hindrance in a system with Z greater than 102 should be described by considering the fragment deformation

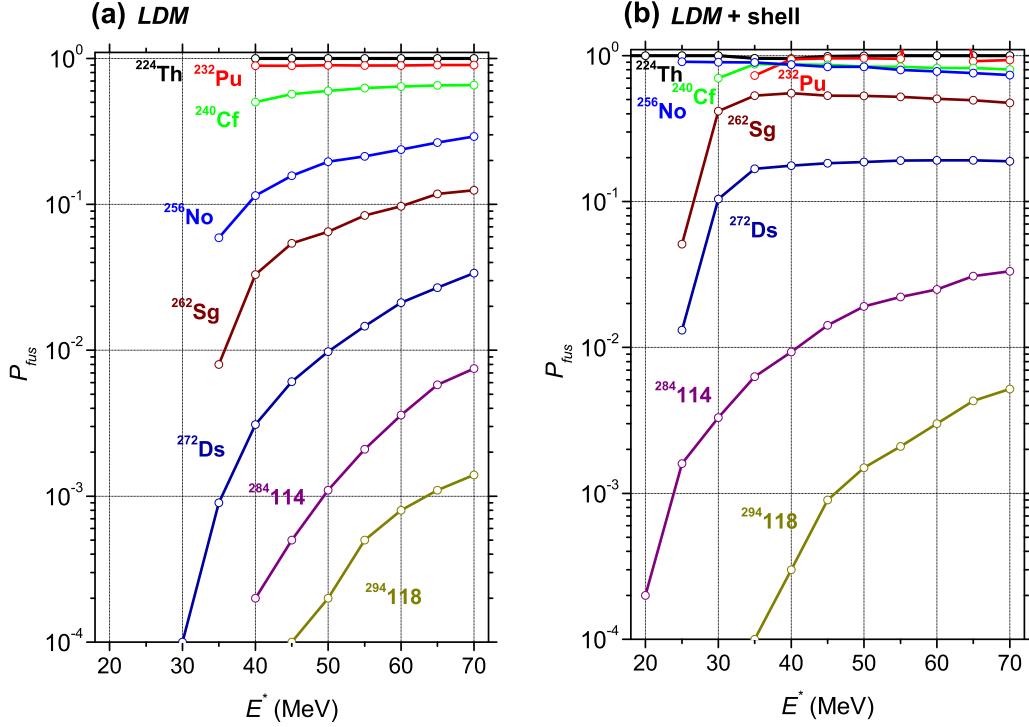


Fig. 6. Fusion probability in the cold fusion reactions calculated by the fluctuation-dissipation model, in the case of angular momentum $l = 0$. The potential energy surface is (a) *LDM* and (b) *LDM + shell* correction energy.

as an important factor.

We assumed that each fragment has the same deformation to avoid the consuming the four-dimensional calculation. We are recognizing that the two deformation parameters are important, especially in the fission process. We need further improvement on this point. It is unclear the temperature dependence of the shell correction energy for very deformed nuclei, especially near the point of contact. We plan to study this problem, and to clarify the influence of the temperature dependence of the shell correction energy on fusion-fission process.

The authors are grateful to Professors Yu. Ts. Oganessian, M.G. Itkis, V.I. Zagrebaev, F. Hanappe and R.A. Gherghescu for their helpful suggestions and valuable discussion throughout the present work. The authors thank Dr. S. Yamaji and his collaborators, who developed the calculation code for potential energy with two-center parameterization. This work has been in part sup-

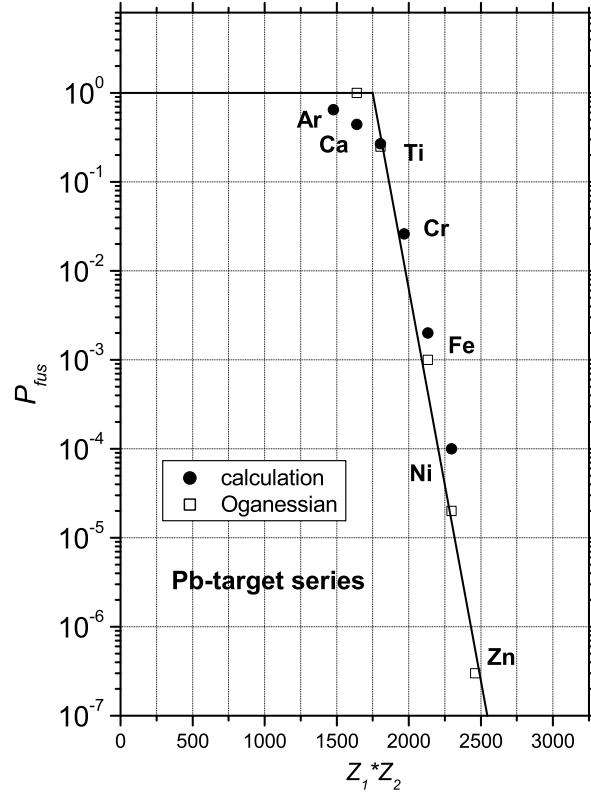


Fig. 7. Fusion probability for Pb-target reaction. We plot the experimental data at the excitation energy corresponding the Bass barrier height by open squares. The calculation in the case of angular momentum $l = 0$ is denoted by solid circles. The name of the element attached to the marks are the projectile.

ported by INTAS projects 03-01-6417.

References

- [1] D. Glas and U. Mosel, Phys. Lett. **49B**, 301 (1974); Nucl. Phys. **A237**, 429 (1975).
- [2] W.J. Swiatecki, Physica Scripta, **24**, 113 (1981); Nucl. Phys. **A376**, 275 (1982).
- [3] S. Bjørnholm and W. J. Swiatecki, Nucl. Phys. **A391**, 471 (1982).
- [4] J.P. Blocki, H. Feldmeier and W.J. Swiatecki, Nucl. Phys. **A459**, 145 (1986).
- [5] J.R.Nix and A.J.Sierk, Phys. Rev. C **15**, 2072 (1977).
- [6] M. Ohta and Y. Aritomo, Phys. Atomic Nuclei **66**, 1026 (2003).
- [7] Y. Aritomo and M. Ohta, Nucl. Phys. **A744**, 3 (2004).
- [8] Y. Aritomo and M. Ohta, Nucl. Phys. **A753**, 152 (2005); nucl-th/0502042.
- [9] J. Maruhn and W. Greiner, Z. Phys. **251**, 431 (1972).

- [10] K. Sato, A. Iwamoto, K. Harada, S. Yamaji, and S. Yoshida, Z. Phys. **A288**, 383 (1978).
- [11] J. Blocki, Y. Boneh, J.R. Nix, J. Randrup, M. Robel, A.J. Sierk and W.J. Swiatecki, Ann. Phys. **113**, 330 (1978).
- [12] J.R. Nix and A.J. Sierk, Nucl. Phys. **A428**, 161c (1984).
- [13] H. Feldmeier, Rep. Prog. Phys. **50**, 915 (1987).
- [14] H.J. Krappe, J.R. Nix, and A.J. Sierk, Phys. Rev. **C20**, 992 (1979).
- [15] S. Suekane, A. Iwamoto, S. Yamaji and K. Harada, JAERI-memo, 5918 (1974).
- [16] A. Iwamoto, S. Yamaji, S. Suekane and K. Harada, Prog. Theor. Phys. **55**, 115 (1976).
- [17] Bock et al., Nucl. Phys. **A388**, 334 (1982).
- [18] R.K. Gupta and W. Greiner, *Heavy Elements and Related New Phenomena* edited by W. Greiner and P.K. Gupta (World Scientific 1999) p. 397.
- [19] P. Moller, J.R. Nix, P. Armbruster, S. Hofmann, G. Munzenberg, Z. Phys. **A356** (1997) 251.
- [20] P. Armbruster, Rep. Prog. Phys., **62** (1999) 465.
- [21] W. Greiner, Proc. of Fusion Dynamics at the Extremes, Dubna, 2000 (World Scientific, Singapore, 2001) p. 1.
- [22] Yu.Ts. Oganessian et al., Nucl. Phys. **A239**, 353 (1975).
- [23] Yu.Ts. Oganessian, Physics of Atomic Nuclei, **63**, 1315 (2000).
- [24] R. Bass, Nucl. Phys. **A231** (1974) 45.

